Vietnam Journal of Catalysis and Adsorption
Tạp chí xúc tác và hấp phụ Việt Nam

https://jca.edu.vn

Green synthesis and characterization of Pluronic coated Zinc nanoparticles from extracts of Tea leaf for antimicrobial activity

Nguyen Thi Huong[1,*], Nguyen Ngoc Son[1], Nguyen Manh Tuong[1], Pham Thi Mai Huong[2], Le Thanh Son[3]

[1] *Institute of Chemistry and Materials, 17 Hoang Sam, Cau Giay, Hanoi, 100000 Vietnam.*
[2] *Hanoi University of Industry, 298 Cau Dien, Bac Tu Liem, Ha Noi, 100000 Vietnam.*
[3] *University of Science, Vietnam National University, Hanoi, 334 Nguyen Trai, Thanh Xuan, Hanoi 100000, Vietnam.*
** Email: nguyenhuong0916@gmail.com*

ARTICLE INFO

Received: 31/03/2024
Accepted: 24/06/2024
Published: 30/12/2024

Keywords:
Zinc oxide nanoparticles;
Pluronic;
antimicrobial activity

ABSTRACT

Zinc oxide nanoparticles (ZnO NPs) are metal oxide materials with potential applications in various industrial and healthcare fields. Recently, they have attracted renewed interest due to the discovery of their unique biological activities. In this study, ZnO NPs were synthesized by a green method and then coated with pluronic. Techniques such as X-ray diffraction (XRD), Fourier transform infrared (FT-IR), scanning electron microscopy (SEM), energy dispersive X-ray (EDX), and dynamic light scattering (DLS) were used to characterize the structure and morphology of the material. The results showed that ZnO NPs synthesized using green tea leaf extract had a particle size in the range of 50-100 nm, spherical shape, and an average crystal size of 21.825 nm. The nanoparticles after surface modification with Pluronic P123 showed a more uniform and stable distribution. The antibacterial activity of the surface-modified nanoparticles was also evaluated against three bacterial strains: *Bacillus subtilis*, *E. coli*, and yeast *S. cerevisiae*. The MIC values obtained for ZnO@P123 in these experiments were 0.3 mg/mL, 0.3 mg/mL, and 0.1 mg/mL, respectively.

Introduction

Recently, the exploration of ZnO NPs' antimicrobial properties has gained significant traction. Studies have demonstrated their potential to counteract a wide range of microorganisms, including bacteria, fungi, and viruses [1-3]. This opens exciting avenues for their use in developing novel antibacterial agents or disinfectants. However, traditional methods of ZnO NP synthesis often involve harsh chemicals or high temperatures, raising concerns about environmental impact and potential cytotoxicity. Green synthesis methods, utilizing natural resources like plant extracts, offer a more sustainable and eco-friendlier alternative [4, 5]. These methods can also influence the size, morphology, and surface properties of the nanoparticles, impacting their functionality. S. Vijayakumar et al. successfully synthesized ZnO NPs from Atalantia monophylla leaf extract [6]. The obtained nanoparticles exhibited a size distribution ranging from 20 to 60 nm, with an average size of 30 nm. Antimicrobial assays were conducted against a range of Gram-positive and Gram-negative bacteria, and the results were evaluated based on the zone of inhibition (ZOI) diameter. The maximum ZOI for ZnO NPs synthesized from A. monophylla was observed against S. aureus (28 mm), followed by E. coli (23 mm), B. cereus (21 mm), P. aeruginosa (22 mm), B. subtilis (20 mm), and K. pneumoniae (19 mm). G. Theophil Anand et al. [7] synthesized ZnO NPs using Prunus dulcis. The synthesized nanoparticles exhibited a hexagonal

https://doi.org/10.62239/jca.2024.070

wurtzite structure with an average particle size of approximately 30 nm. The antibacterial activity test results obtained on some bacteria were quite good such as E. coli (32 mm), S. aureus (18 mm).

Tea leaves contain nearly 4,000 different types of biological active ingredients, one-third of which are polyphenol derivatives, mainly flavonoids. Other compounds present in tea are alkaloids such as caffeine, theophylline and theobromine), amino acids, carbohydrates, proteins, chlorophyll, fluoride, etc.[8-10]. Due to the presence of appealing phytochemical components, tea leaf extract has been extensively utilized in numerous studies to produce different types of nanoparticles, including metal nanoparticles: iron (Fe) [11], silver (Ag) [12, 13] and metal oxide nanoparticles such as magnetite (Fe_3O_4) NPs [14], copper oxide (CuO) [15, 16].

This study explores the green synthesis of ZnO NPs using extracts from Camellia sinensis (tea) leaves. Additionally, the synthesized ZnO NPs were further encapsulated with Pluronic, a biocompatible polymer. Pluronic coating can enhance the stability of the nanoparticles in aqueous environments, potentially improving their dispersion and biocompatibility. Following synthesis, various characterization techniques were employed to analyze the structure, morphology, and size distribution of the Pluronic-coated ZnO NPs. Subsequently, the antimicrobial activity of the synthesized nanoparticles was evaluated against a panel of bacterial strains (Bacillus subtilis and E. coli) and a yeast strain (Saccharomyces cerevisiae). This investigation aimed to assess the effectiveness of the Pluronic coating in modulating the stability and antimicrobial efficacy of the green-synthesized ZnO NPs.

Experimental

Chemicals

Zinc acetate dihydrate ($Zn(CH_3COO)_2.2H_2O$, Merck) is the zinc precursor, Pluronic P123 (5.800 Da, Sigma-Aldrich) is the encapsulating agent. Anhydrous Ethanol (EtOH, Emsure), Deionized Water (DI, TDS<5) were used as the extraction medium.

Preparation of green tea leaf extract

Fresh green tea leaves were gathered, and any leaves that were damaged, infested with insects, or decaying were discarded. Prior to drying at a temperature of 60°C for a duration of 24 hours, the leaves underwent two rounds of thorough washing using clean water. The dry leaves were pulverized into a fine powder and subjected to extraction using a solvent mixture of ethanol and deionized water (EtOH/DI, 1:1 v/v) at a temperature of 60°C for a duration of 2 hours. Subsequently, the extract was strained using a silk filter to eliminate any remaining solid particles. The suspended particles were removed using centrifugation at a speed of 5000 revolutions per minute for a duration of 5 minutes in order to produce the extract of green tea leaves. The given sample was refrigerated at a temperature of 5°C for further investigation.

Synthesis of ZnO NPs

The process is similar to our previous publication [17]. 50 mL of green tea extract was mixed with 100 mL of deionized water in a 250 mL Erlenmeyer flask. Zinc acetate dihydrate (3.0 g) was dissolved in 50 mL of deionized water in another flask. The synthesis reaction of ZnO nanoparticles was conducted using ultrasonic assistance. The green tea leaf extract underwent sonication, while the zinc precursor solution was introduced into the reaction mixture using a peristaltic pump at a flow rate of 5 mL/min. After completely consuming the precursor solution (about 10 minutes), the reaction continued for a further 10 minutes before the sonication was stopped. The resultant solid from the reaction was isolated using centrifugation at a speed of 10,000 revolutions per minute for a duration of 5 minutes, followed by drying at a temperature of 50 °C for a period of 8 hours. The solid obtained was coarsely pulverized prior to undergoing calcination at a temperature of 600 °C for a duration of 2 hours, resulting in the production of fine, white powdered ZnO nanoparticles.

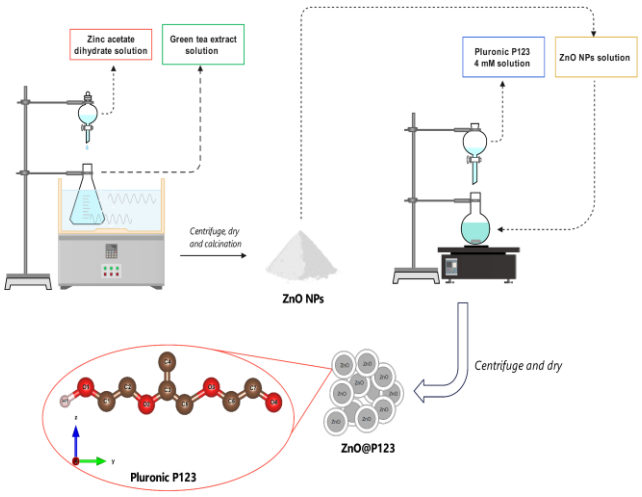

Scheme 1: Synthesis process of ZnO NPs and ZnO@P123

https://doi.org/10.62239/jca.2024.070

Modification of ZnO surface with Pluronic P123

Disperse 1 g of the as-prepared ZnO NPs in 100 mL of the EtOH:DI (1:1 v/v) solvent mixture using ultrasonication for 5 minutes. Transfer the entire dispersion to a 250 mL round-bottom flask. In a separate Erlenmeyer flask, prepare 100 mL of a Pluronic P123 4 mM solution in DI water. Load the P123 solution into a pressure-equalizing dropping funnel. Conduct the reaction under magnetic stirring at room temperature (average stirring speed: 300 rpm) for 24 hours. Add the P123 solution from the dropping funnel at a controlled rate of 1 mL/minute. After the reaction was complete, recover the solid fraction by centrifugation (10,000 rpm, 5 minutes). Wash the centrifuged solid three times with DI water using ultrasonication to remove any unreacted P123. Dry the washed product in an oven at 50°C for 12 hours to obtain the ZnO@P123 (Scheme 1).

Characterization of nanoparticles

Field emission scanning electron microscopy (FESEM, Jeol-JMS 6490) and scanning electron microscopy (SEM; Hitachi S-4800) were used to examine the structural morphologies of both bare and Pluronic P-123-coated ZnO NPs. Energydispersive X-ray spectroscopy (EDX) was applied to determine the surface relative atomic percentage. The structural crystallinity of both nanoparticles was analyzed using a diffractometer (PANalytical X'Pert PRO X-ray). The functional groups of bare and coated ZnO NPs were characterized using Fourier transform infrared spectroscopy (FTIR, TENSOR II, Bruker) by potassium bromide (KBr) method.

Evaluation of the antimicrobial

The antibacterial activity of ZnO@P123 was determined by the minimum inhibitory concentration (MIC) value using the disc diffusion method [18]. Briefly, 37.0 g of nutrient agar was dissolved in 1,000 mL of distilled water. It was then sterilized in an autoclave at 121°C/7 kg for 20 minutes. The nutrient agar was then poured into sterile petri dishes and allowed to solidify. The specific bacterial strains were cultured in the nutrient medium and spread evenly over the surface of the agar plate using a sterilized L-shaped glass rod. ZnO@P123 was added to the agar suspension at different concentrations and allowed to cool until gelled. The plates were incubated at 37°C/24h. The MIC value of ZnO@P123 was then determined visually, and the MIC was the lowest concentration of ZnO@P123 observed to inhibit the growth of the bacterial strains.

Results and discussion

Synthesis of ZnO NPs using green tea extract

The infrared spectrum of ZnO NPs synthesized using green tea leaf extract is shown in Fig. 1(a). The absorption peaks at 453 cm^{-1} correspond to the Zn-O bond, while the broad peak at 3430 cm^{-1} corresponds to the O-H bond of water absorbed on the surface of ZnO NPs, which are fundamental features of zinc oxide material. Furthermore, there are numerous additional absorption peaks that can be detected at the position of 1625 cm^{-1}, which is indicative of the presence of the C=O bond, and at 1120 cm^{-1}, which is characteristic of the C-OH bond found in phytochemical substances present in the extract. The involvement of physiologically active chemicals found in green tea leaf extract in the formation of zinc oxide nanoparticles is evident.

The X-ray diffraction (XRD) results for the determination of ZnO NPs may be found in Fig. 2(a). The diffraction peaks observed at the 2theta diffraction angles are 31.8°, 34.41°, 36.28°, 47.55°, 56.59°, 62.89°, 66.42°, 67.96°, and 69.09°. These peaks correspond to the diffraction planes (100), (002), (101), (102), (110), (103), (112), and (201) of the ZnO crystal hexagonal wurtzite structure. These observations match with the PDF 01-071-6424 pattern. The XRD spectrum exhibits distinct and slender diffraction peaks, suggesting that the produced nanoparticles possess a high level of purity and crystalline structure.

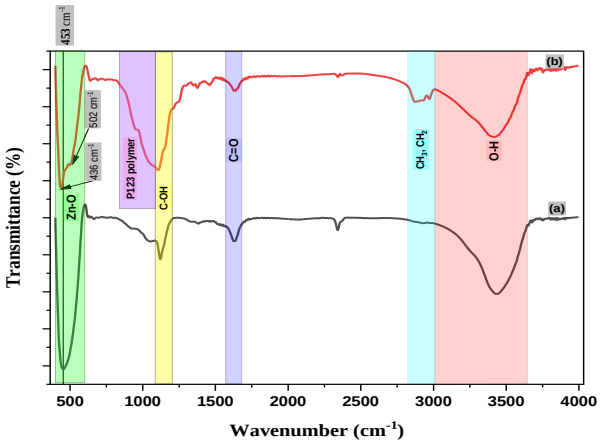

Fig. 1: FTIR spectra of ZnO NPs (a) and ZnO@P123 (b)

The average crystal size is determined using the Scherrer equation. Where, K is Scherrer's constant, which is equal to 0.94 for spherical crystals of ZnO nanoparticles and using a CuKα radiation source with a wavelength of 1.5406 Å. The results indicate that the majority of the crystal sizes, as determined from the diffraction peaks, fall within the range of 19-22 nm.

https://doi.org/10.62239/jca.2024.070

However, it should be noted that the crystal size calculated at the (103) crystal plane is significantly larger, measuring 31.055 nm. The determined mean crystal size is 21.825 nm.

The SEM (Fig. 3a) results indicate that the particles exhibit a rather homogeneous size distribution, with the majority of particles displaying a spherical morphology. Particle clustering into huge clusters is observed. Furthermore, the TEM images (Fig. 3b) at the right provide confirmation of the sphericsal morphology of the particles. The estimation of particle size ranges from approximately 50 to 100 nanometers and the image exhibits a distinct contrast, allowing for the observation of clear boundaries between nanoparticles.

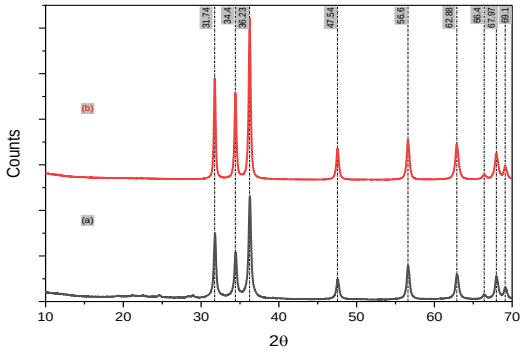

Fig. 2: XRD patterm of ZnO NPs (a) and ZnO@P123 (b)

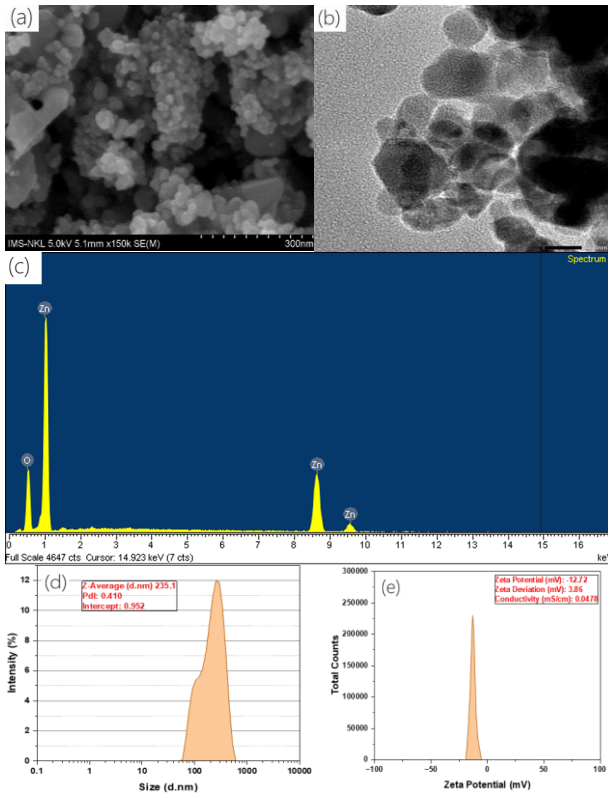

Fig. 3: SEM (a), TEM (b) images, EDX (c) and distribution of hydrodynamic size (d) and zeta potential (e) of ZnO NPs

The EDX spectrum of ZnO NPs (Fig. 3c). Only the energy diffraction peaks corresponding to the elements zinc (Zn) and oxygen (O) are seen on the EDX spectrum, while no energy diffraction peaks for any other elements are detected. This indicates that the ZnO nanoparticles generated in their original state are of exceptional purity.

The hydrodynamic diameter and zeta potential of the nanoparticle surface are determined as shown in Fig. 3d. Accordingly, the dynamic size of nanoparticles is distributed in the range from more than 50 nm to more than 500 nm. Which is mainly concentrated in the region 190 nm to 340 nm. The observed particle size is much larger than that obtained from the electron microscope. This can be attributed to the clustering of some nanoparticles in the aqueous medium to form clusters of larger size. In addition, it can be seen that in the SEM image the uniformity is only at a good level, and some nanoparticles with large irregular sizes can be observed. It is possible that they also contribute to the results of particle size distribution obtained as determined by DLS. The nanoparticle surface zeta potential was also determined to be about -12.72 mV (Fig. 3e). The zeta potential amplitude is quite large, which shows that the nanoparticle has quite good stability.

Surface modification of ZnO NPs with Pluronic P-123

The Fourier transform infrared (FTIR) spectrum of the surface modified ZnO NPs by Pluronic P123 (ZnO@P123) is shown in Fig. 1(b). It can be clearly observed that the spectrum exhibits all the characteristic absorption peaks of ZnO NPs, especially the very characteristic peak at the wavenumber range of 450 cm^{-1} to 500 cm^{-1} representing the Zn-O bond. The characteristic peaks of water molecules adsorbed on the surface of nanoparticles as well as active substances in the extract present in the nanoparticles are also observed. Notably, the absorption peak at 453 cm^{-1} of ZnO now almost degenerates into a peak at 435 cm^{-1} and a shoulder at 502 cm^{-1}. This splitting can be attributed to the effect of P123 being attached to the surface of the nanoparticles. Another notable point in the FTIR spectrum of ZnO@P123 is the appearance of a strong absorption band in the range of 850 cm^{-1} to 1080 cm^{-1} with a shoulder at around 950 cm^{-1}, which is the characteristic absorption band of P123 polymer [19]. Thus, the FTIR spectrum showed the successful attachment of P123 onto ZnO NPs.

The XRD pattern of ZnO@P123 is also presented in Fig. 2(b). The diffraction peaks of ZnO@P123 are similar to those of ZnO NPs, with almost no shift in the diffraction

https://doi.org/10.62239/jca.2024.070

angles. This demonstrates that the surface modification of ZnO NPs by P123 does not change their crystal structure.

The morphology of ZnO@P123 was observed through SEM and TEM images as shown in Fig. 4a and Fig. 4b. The SEM results showed a clear morphological change of ZnO after surface modification with P123. Specifically, the nanoparticles agglomerated into larger clusters. The particle diameter also appeared to increase.

The results of elemental composition analysis by EDX spectrum (Fig. 4c). In addition to oxygen (O) and zinc (Zn), the elemental also includes a significant amount of carbon (C), with values of 5% by mass and 12.56% by number of atoms. This indicates the presence of P123 in quite significant amounts, which supports the assertion that P123 was successfully attached to the ZnO NPs surface.

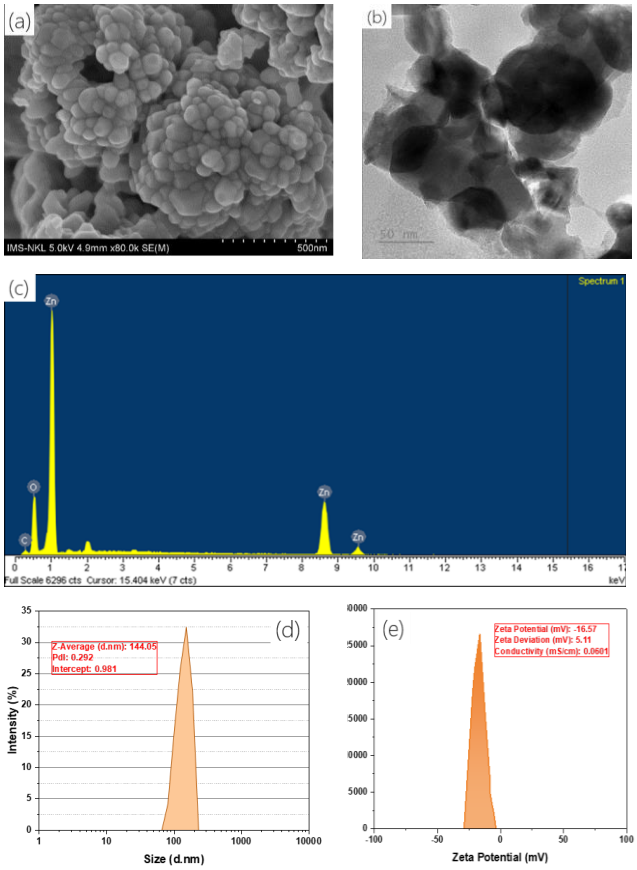

Fig. 4: SEM (a), TEM (b) images, EDX (c) and distribution of hydrodynamic size (d) and zeta potential (e) of ZnO@P123

The hydrodynamic size distribution of ZnO@P123 is shown in the graph of Fig. 4d. The results show that the Z-Average value is 144.05 nm and the PdI is 0.292. Compared to the corresponding values of ZnO NPs, it shows that after surface modification with P123, the hydrodynamic diameter of the nanoparticles decreased and became more uniform. This observation is also consistent with the results of zeta potential determination of ZnO@P123 presented in Fig. 4e . The zeta potential decreased to -16.57 mV, which is more negative than that of ZnO NPs. This explains the better dispersion and stability of ZnO@P123.

Antibacterial Activity Test

The ZnO-P123 content was evaluated at concentrations of 0.1, 0.3, 0.5, 1.0, and 3.0 for the three bacterial strains under investigation. The findings indicated a progressive decline in bacterial density with an increasing ZnO-P123 level. Specifically, when the concentration of ZnO-P123 reached 0.3 mg/mL, a noticeable reduction in the population of E.coli bacteria was detected. Meanwhile, the concentrations of 0.3 mg/mL and 0.1 mg/mL of bacteria B. subtilis and S. cerevisiae, respectively, resulted in a noticeable drop in the quantity of bacteria.

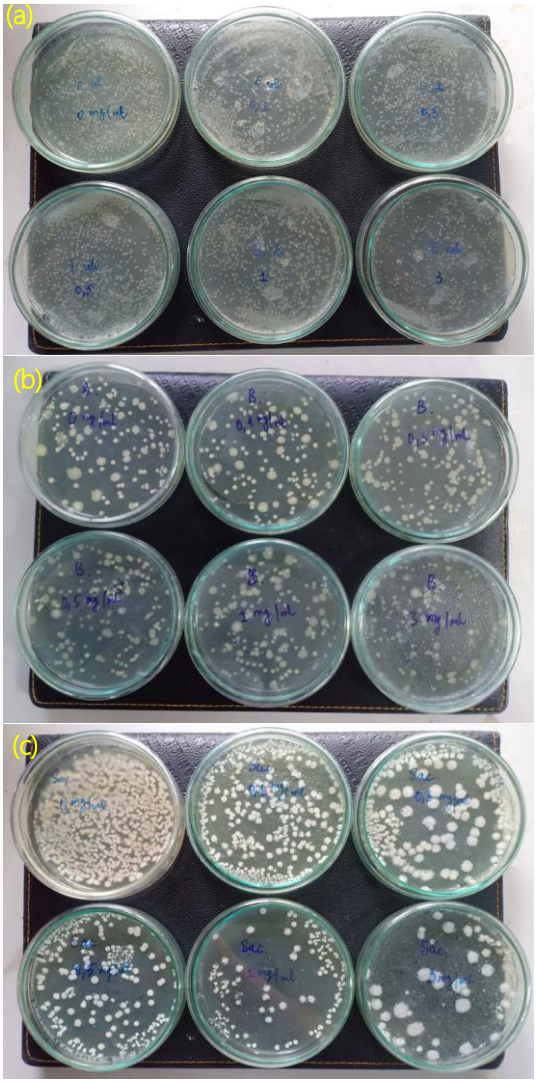

Fig. 5: Antibacterial efficacy of ZnO@P123 against S. cerevisiae (c), B. subtilis (b), and E. coli (a) at varying doses

The minimum inhibitory concentration (MIC) values of ZnO-P123 for the three bacterial strains examined, namely E. coli, B. subtilis, and S. cerevisiae, are 0.3 mg/mL, 0.3 mg/mL, and 0.1 mg/mL, respectively. The results indicate that ZnO-P123 exhibits a significant antibacterial action, particularly against the S. cerevisiae bacterial strain. This result suggests the potential use of ZnO-P123 in antibacterial activities.

The antibacterial mechanism of ZnO-NPs is not fully understood, but it is thought to involve multiple factors, including the release of zinc ions, the generation of reactive oxygen species (ROS), and the disruption of bacterial cell membranes. Zinc ions can interfere with bacterial enzymes and DNA replication, while ROS can damage cellular components. The disruption of bacterial cell membranes can lead to leakage of cellular contents and cell death.

The observed differences in the MIC values of ZnO-P123 for the three bacterial strains may be due to variations in their cell wall structures and susceptibility to ZnO-NPs. E. coli and B. subtilis have a Gram-negative cell wall, which is more resistant to the action of ZnO-NPs than the Gram-positive cell wall of S. cerevisiae.

Conclusion

The results of this study demonstrate that green tea leaf extract is an effective agent for the synthesis of ZnO NPs. The as-prepared nanoparticles have a spherical shape, a crystal size of 21.825 nm, and a particle size of 50-100 nm, which are suitable for biomedical applications. However, the DLS results showed that they were unstable and had relatively poor dispersibility. Surface modification of ZnO NPs with the surface-active agent Pluronic P123 overcame these drawbacks. The surface-modified nanoparticles were evaluated for antibacterial activity against three bacterial strains: E. coli, B. subtilis, and yeast S. cerevisiae, with positive results. This result shows the potential application of ZnO-P123 in the antibacterial field such as antibacterial bandages, antibacterial fabrics, antibacterial drugs in hospitals, or antibacterial skin creams.

Acknowledgments

This research has received financial support from the Institute of Chemistry and Materials.

References

1. P.K. Mishra, H. Mishra, A. Ekielski, S. Talegaonkar, B. Vaidya, Drug Discovery Today 22 (2017) 1825. https://doi.org/10.1016/j.drudis.2017.08.006
2. P.J.P. Espitia, N.d.F.F. Soares, J.S.d.R. Coimbra, N.J. de Andrade, R.S. Cruz, E.A.A. Medeiros, Food and Bioprocess Technology 5 (2012) 1447. https://doi.org/10.1007/s11947-012-0797-6
3. A. Moezzi, A.M. McDonagh, M.B. Cortie, Chemical engineering journal 185 (2012) 1. https://doi.org/10.3390/pr11041193
4. V.V. Makarov, A.J. Love, O.V. Sinitsyna, S.S. Makarova, I.V. Yaminsky, M.E. Taliansky, N.O. Kalinina, ActaNaturae 6 (2014) 35. https://doi.org/10.32607/20758251-2014-6-1-35-44
5. S. Iravani, Green Chemistry 13 (2011) 2638. https://doi.org/10.1039/C1GC15386B
6. S. Vijayakumar, S. Mahadevan, P. Arulmozhi, S. Sriram, P.K. Praseetha, Materials Science in Semiconductor Processing 82 (2018) 39. https://doi.org/10.1016/j.mssp.2018.03.017
7. G. Theophil Anand, D. Renuka, R. Ramesh, L. Anandaraj, S. John Sundaram, G. Ramalingam, C.M. Magdalane, A.K.H. Bashir, M. Maaza, K. Kaviyarasu, Surfaces and Interfaces 17 (2019) 100376. https://doi.org/10.1016/j.surfin.2019.100376
8. T. Mahmood, N. Akhtar, B.A. Khan, Journal of Medicinal Plants Research 4 (2010) 2028. https://doi.org/10.5897/JMPR10.010
9. C. Cabrera, R. Giménez, M.C. López, Journal of Agricultural and Food Chemistry 51 (2003) 4427. https://doi.org/10.1021/jf0300801
10. B.E. Sumpio, A.C. Cordova, D.W. Berke-Schlessel, F. Qin, Q.H. Chen, J Am Coll Surg 202 (2006) 813. https://doi.org/10.1016/j.jamcollsurg.2006.01.018
11. K. Gottimukkala, R. Harika, D. Zamare, J. Nanomed. Biother. Discov 7 (2017) 151. https://doi.org/10.4172/2155-983X.1000151
12. K. Tran Khac, H. Hoang Phu, H. Tran Thi, V. Dinh Thuy, H. Do Thi, Heliyon 9 (2023) e20707. https://doi.org/10.1016/j.heliyon.2023.e20707
13. S. Onitsuka, T. Hamada, H. Okamura, Colloids and Surfaces B: Biointerfaces 173 (2019) 242. https://doi.org/10.1016/j.colsurfb.2018.09.055
14. A. Jawed, A.K. Golder, L.M. Pandey, Bioresource Technology 376 (2023) 128816. https://doi.org/10.1016/j.biortech.2023.128816
15. L. Dou, X. Zhang, M.M. Zangeneh, Y. Zhang, Bioorganic chemistry 106 (2021) 104468. https://doi.org/10.1016/j.bioorg.2020.104468
16. J. Emima Jeronsia, L. Allwin Joseph, P. Annie Vinosha, A. Jerline Mary, S. Jerome Das, Materials Today: Proceedings 8 (2019) 214. https://doi.org/10.1016/j.matpr.2019.02.103
17. N.N. Son, V.M. Thanh, N.T. Huong, ChemistrySelect 8 (2023) e202303214. https://doi.org/10.1002/slct.202303214
18. T.M.H. Pham, N.S. Nguyen, T.N. Dao, T.T. Le, T.H. Nguyen, H.N. Pham, T.H. Nguyen, Journal of Nanomaterials 2022 (2022) 2485291. https://doi.org/10.1155/2022/2485291
19. T. Bala, R.D. Gunning, M. Venkatesan, J.F. Godsell, S. Roy, K.M. Ryan, Nanotechnology 20 (2009) 415603. https://doi.org/10.1088/0957-4484/20/41/415603